Nd:YAG laser hardening of AISI 410 stainless steel: microstructural evaluation, mechanical properties, and corrosion behavior

Mahmoud Moradi[1, 2], Davud Ghorbani[2, 3], Mojtaba KaramiMoghadam[1, 2], Mahdi Kazazi[2, 4], Fardin Rouzbahani[3], Shadi Karazi[5]

[1] Department of Mechanical Engineering, Faculty of Engineering, Malayer University, Malayer, Iran
[2] Laser Materials Processing Research Center, Malayer University, Malayer, Iran
[3] Department of Mechanical Engineering, Faculty of Engineering, Islamic Azad University of Hamedan Branch, Hamedan, Iran
[4]Department of Materials Engineering, Faculty of Engineering, Malayer University, Malayer, Iran
[5]School of Mech. & Maun. Eng., Dublin City University, Dublin, Ireland

Abstract:

In this paper, a pulsed Nd:YAG laser with a maximum power of 700 W, was utilized to investigate the laser surface hardening of AISI 410 martensitic stainless steel. Focal point position, scanning speed and pulse width were considered as process variable parameters. Corrosion behavior of laser surface hardened samples were investigated by IVIUMSTAT apparatus in a 3.5wt% NaCl solution. Maximum microhardness, depth, and width of hardness and percentage of ferrite phase of metallographic and FESEM pictures were evaluated. Results show that surface hardness increased up to 762 HV. Results also reveal that the laser focal point position and pulse width are effective parameters in laser hardening process. In potentiodynamic polarization tests potential stated to increase at a rate of 1 mV/s from -0.4 V to 0.2 V. Results indicate that the corrosion resistance increased due to laser hardening process.

Keywords: laser surface hardening; Nd:YAG laser; electrochemical tests; corrosion.

1- Introduction

Laser hardening is a new method for local and precise hardening. Martensite is a hard phase which is necessary for surfaces exposed to wear. Surface hardening goal is to achieve a hard thin layer on the metal surface whereas internal sections remained unchanged and tough. In laser surface hardening, the surface warms up to austenite temperature region, and after the cooling process, the martensite phase will form [1, 2]. In this method, distortion is less than other hardening processes such as induce and flame hardening.

AISI 410 is one of the most common industrial steels. It is used in pump gates and impellers, tools and pressure vessels due to its wear and corrosion resistance and capability of heat treatment. Laser applications and their advantages made it be used in laser welding, laser cutting, and laser hardening. Simultaneous effects of wear and corrosion have shortened AISI 410 life; therefore, it is necessary to improve its performance with several surface treatments. Mahmoudi et al. [3] studied surface hardening of AISI 410 martensitic stainless steel by pulsed solid state Nd:YAG laser with maximum power of 400 W. The goal of this study was calculating the depth of hardness resulted from constant power of 300 W, constant pulse width of 20 ms and changing other parameters such as laser scanning speed (1-4 mm/s) and focal point position (10-6 mm). They found that low focal point position will lead to surface melting and dissolves carbides in grains. The value of hardness achieved in their research was 2.5 times

more than that obtained by flame hardening. Al-Sayed et al. [4] studied on wear and corrosion behavior of hardened AISI 416 with different powers and scanning speeds. They showed that corrosion behavior of AISI 416 is related to two factors, including a) amount and size of carbides and magnesium sulfide impurities in grain boundaries and b) microstructure. As the amount of trapped chromium in carbides increases, the formation of a passive layer happens harder. Zirepour et al. [5] studied on corrosion behavior of AISI 420 hardened by Nd:YAG laser. Jahromi et al. [6] studied the effect of different pre-heat treatment processes on the hardness of AISI 410; surface treated using Nd:YAG laser for fine ferrite, fine and coarse martensite microstructures, which the results showed that surface treatment by laser increased the hardness of all three microstructures. The achieved hardness was 700 HV, and corrosion resistance increased to a significant level where corrosion current density reported 113 $\mu A/cm^2$. Krishna et al. [7] studied on fatigue properties of LENS-treated AISI 410. They found that an increase in the amount of retained austenite in the microstructure will reduce the final hardness. Also, they showed that the retained austenite is highly related to laser power and scanning speed. Retained austenite is one of the most significant factors affecting the corrosion behavior of martensitic steels. Numerical and experimental analyses of the laser surface hardening with overlapped tracks to design the configuration of the process for AISI 410 were done by Cordovilla et al. [8]. Badkar et al. [9] worked on optimization for calculating the geometrical dimensions of the hardened area via response surface method and hardening 17 samples of titanium by solid-state Nd:YAG laser. They found that the width of the hardened area and angle of hardening will increase by reducing laser scanning speed and increasing laser power. Many researchers investigated laser surface hardening by Nd:YAG laser with a vriety of inputs. Soriano used it for studying microstructure, residual stress and mechanical properties of austempered ductile iron [10]; Jong-Do et al. employed it to invistigate the microstructure of low carbon steels after hardening process [11]; Lo et al. studied the effect of laser scanning speed on laser hardening of AISI 440C [12]; Babu et al. studied hardening of low alloy steel EN25 to achieve optimized parameters to increase hardness [13]; and Pinahin et al. laser hardening of tools steels and perform wear test on them [14].

In this research, Nd:YAG laser is used to improve the surface hardness of AISI 410 martensitic stainless steel. The effects of Focal point position, scanning speed and pulse width on hardness, the geometrical dimension of the hardened zone, metallographic phases, and corrosion behavior of laser hardened sample in 3.5 wt% NaCl solution were studied. The goal of this study is to achieve a hard and corrosion resistant surface. Schematic of the hardening process and corrosion tests is shown in Figure 1.

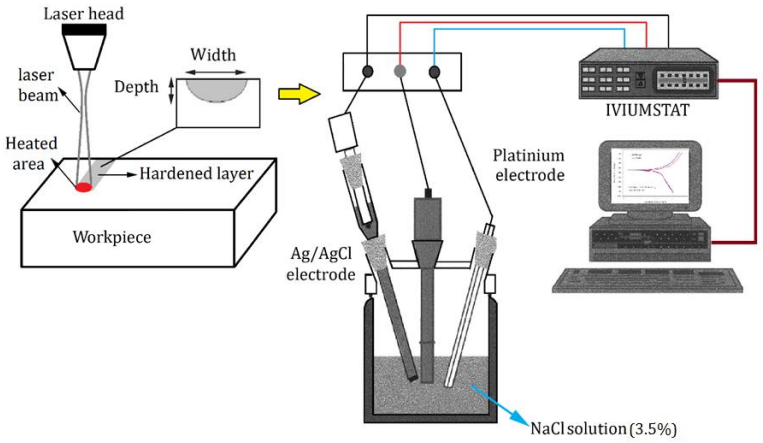

Fig. 1. Schematic of the hardening process and corrosion tests of AISI 410 [15, 16]

2- Empirical experiments

2-1 laser and material

The material used in this research was AISI 410 martensitic stainless steel with the chemical composition mentioned in Table 1. The chemical composition measured by Quantometer at laboratory conditions at 28 °C and humidity of 14 percent.

Table 1. The chemical composition of AISI 410 (wt %)

Element Name	C	Mo	Cr	Cu	S	P	Mn	Ni	Si	Al	V	Fe
Weight percent	0.15	0.03	013.5	0.11	0.02	0.02	0.51	0.12	0.28	0.01	0.02	Balance

The microstructure of the untreated sample is a martensitic base with a uniform distribution. The samples were prepared from a 50 mm diameter rod and machined to a thickness of 10 mm by turning and grinding.

Nd:YAG laser with a maximum power of 700 W used for surface hardening. Experimental settings of the experiments listed in Table 2. As shown in Table 2 in F series the focal point position changes from 22 to 28 mm. In E series by changing average power and pulse width, pulse energy varies from 14.7 to 17.85 J. The goal of E series tests is to keep peak power constant on a number equal to those for F series, and changing pulse energy which obtained by simultaneous change of average power and pulse width according to Equations 1 and 2 [17]:

$$E = \frac{P_{Average}}{F_{Pulse}} \quad (1)$$

$$P_{Peak} = \frac{E}{W_{Pulse}} \quad (2)$$

Where E is pulse energy (J), $P_{average}$ is average power (W), F_{pulse} is pulse frequency (Hz), P_{peak} is peak power (kW), and W_{pulse} is pulse width (ms).

Table 2. Experimental settings of Nd:YAG laser

Input Parameters									
NO	Samples	Laser Pulse Frequency (Hz)	Average Power (W)	F.P.P (mm)	Scanning Speed (mm/s)	Current (A)	Pulse width(ms)	Ep (J)	Peak Power (kW)
1	F1	15	285	28	2	150	18	19	1.055
2	F2	15	285	26	2	150	18	19	1.055
3	F3	15	285	24	2	150	18	19	1.055
4	F4	15	285	22	2	150	18	19	1.055
5	E1	15	268	24	2	150	17	17.85	1.055
6	E2	15	252	24	2	150	16	16.8	1.055
7	E3	15	236	24	2	150	15	15.75	1.055
8	E4	15	220	24	2	150	14	14.7	1.055

In E series, tests energy intensity is constant along the path for each pulse. In these tests by decreasing the pulse width of the laser beam, sharper pulses will interact on a matter which increases absorption rate and efficiency of the laser. Accessible parameters of laser apparatus were pulse frequency of 1-1000 Hz, pulse width of 0.2-20 ms and pulse energy of 0-40 J. It is noticeable that every combination of these parameters was not attainable, because average power could not exceed 700 W. The pulsed laser hardening with low pulse frequencies enables a higher depth in hardening compared with continuous wave laser hardening [18]. In this present study, the effect of focal point position and pulse width is studied on the corrosion behavior while the laser intensity is constant.

To develop the metallurgical samples, the hardened samples (after the laser hardening process) were cut, mounted and polished. To find out the distribution of hardness, the hardened layer surface cross-sectional depth and width microhardnesses were measured utilizing the Barreiss V-test microhardness device. Three microhardness estimations were measured and averaged for each hardened sample. These measurements were taken by applying a 300G load and a 30s dwell time (according to ASTM E92-17). For metallography, samples etched in a reagent solution of 15cc Hydrochloric acid, 10cc Acetic acid and 10cc Nitric acid [19].

Images of samples after metallography were made by Leica MEF 4A optical microscope with a magnification of 50X and 100X. For measuring the geometrical dimensions of the hardened area, the ImageJ software has been utilised. Optical microscopy (OM) and Field Emission Scanning Electron Microscopy (FE-SEM) were employed to analyze the microstructure of the hardened zone, and the percentage of ferrite phase in the center of the hardened area utilising Clemex software.

2-2 Corrosion test

Corrosion behavior of AISI 410 samples was studied in 3.5 wt% NaCl solution in ambient temperature by potentiodynamic polarization measurements. The exposed area of samples for

corrosion tests was 3*10 mm^2. The all electrochemical tests conducted by an IVIUM electrochemical workstation, with an auxiliary electrode of platinum and a reference electrode of Ag/AgCl. In potentiodynamic polarization measurement, the potential increased at a rate of 1 mV/s from -0.4 to 0.2 V (vs. OCP).

3- Results and discussion

In this paper, the effects of Nd:YAG laser parameters (i.e., focal point position and pulse energy) on AISI 410 martensitic stainless steel in surface hardening process were investigated. To study surface properties, geometrical dimensions of the hardened layer (width and depth of penetration), microhardness distribution in depth and width of laser hardening, microstructures and ferrite phase percentage in the centerline of the hardened area were analyzed at three locations and average values were recorded (Table 3). Corrosion behavior of laser hardened sample in 3.5 wt% NaCl solution was studied as well.

Table 3. Responses from laser hardening of Nd:YAG laser

	Responses			
Samples	Hardness (HV)	Depth (µm)	Width (µm)	Ferrite percent (%)
F1	355	130	3047	5.87
F2	417	140	3035	2.08
F3	444	199	3011	1.8
F4	520	270	3312	1.4
E1	762	460	3918	0.54
E2	747	350	2107	0.78
E3	598	211	2188	0.85
E4	546	142	2208	1.2

3-1 Geometrical dimensions of the hardened area

Gaussian distribution model of the laser beam is shown in Figure 2 [20-22]. As shown in Figure 2(a) in Gaussian model laser heat input at the center of the laser beam is more than the corners and by moving from the center toward the corners, energy intensity of laser decreases. Also in Figure 2(b) by increasing the distance from the laser beam focal plane, Z_r, energy intensity decreases and beam divergence increases the laser beam diameter. In this paper increases in focal distance means moving away from the focal plane.

These issues have a direct influence on both laser beam penetration depth and hardness of the laser affected area. Surface melting because of higher heat input increases hardness and its depth and width, but these samples are not desirable in laser hardening process. It should be noted that in sample #F1 due to excess (more than enough) distance between laser and surface, width and depth of penetration decreased.

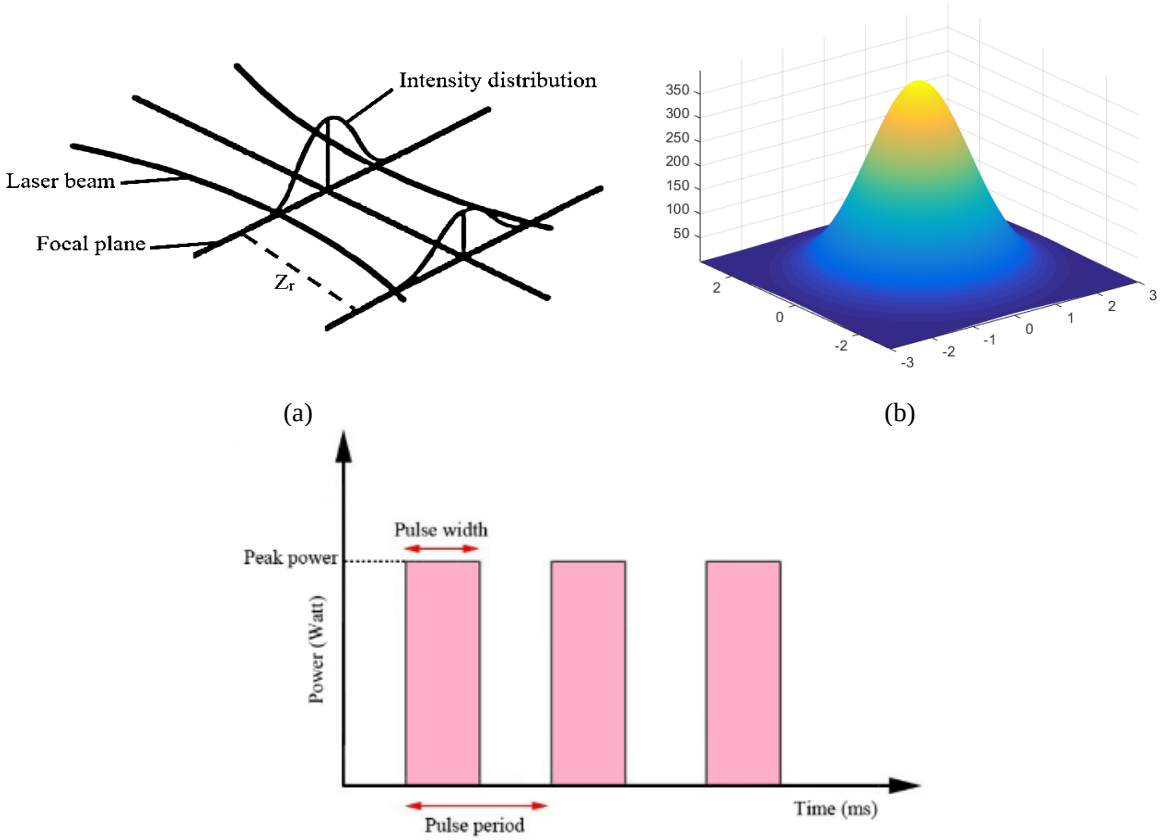

Fig. 2.a) Schematic of Gaussian distribution **b)** normal Gaussian distribution **c)** schematic of Nd:YAG laser pulse diagram [20-22]

In Figure 3 macro metallographic image of sample F3 and F1 affected by laser focal point position and also sample E2, are shown.

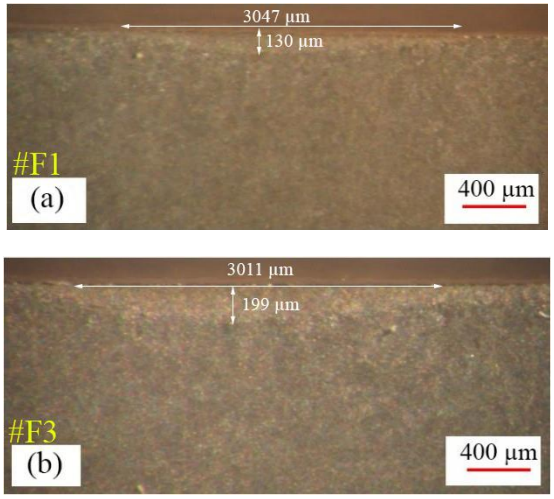

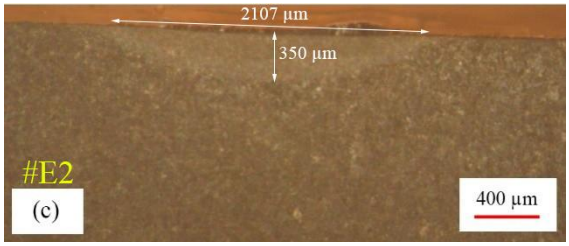

Fig. 3 Cross section of laser hardened area a) sample F1 b) sample F3 c) sample E2

In Figure 3 difference between depth and width of the hardened layer for samples F1, F3 and E2 which were affected with different focal point position and pulse energy are shown. For sample F1 which had a higher focal point distance of 28 mm, depth of penetration is 130 µm while the width of the hardened layer is 3047 µm. For sample F3 with a smaller focal point distance of 24mm, deeper depth and smaller width were affected, and for sample E2 with a higher pulse energy of 16.8 J and a smaller focal point position in comparison with sample F1, depth of diffusion was 350 µm.

3-2 Study of microhardness distribution

Certainly, changes in the laser focal point position affect microhardness. Figure 4 shows microhardness changes from the surface to the depth for samples F1 to F3. It is clear that in sample F3 surface, hardness increased up to 444 HV due to laser surface hardening.

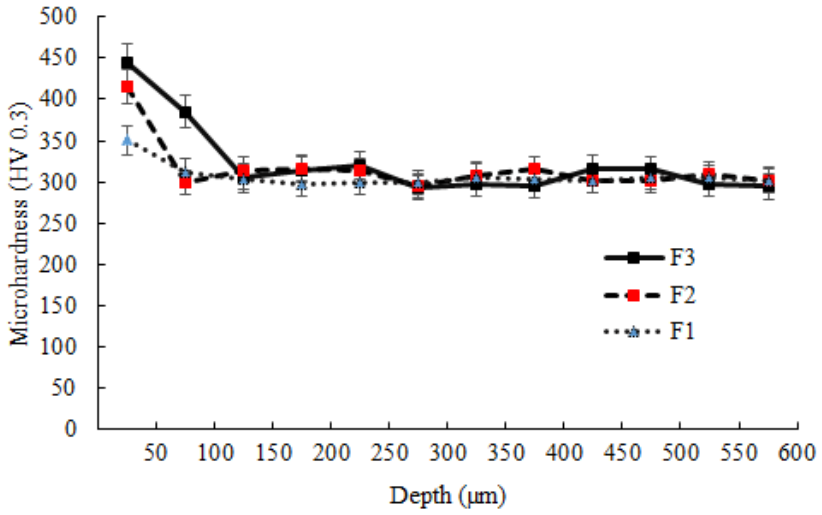

Fig. 4 Microhardness profile in depth of the laser-hardened layer in focal point position tests

Focal point position has a direct effect on the depth of the surface laser hardening layer [23]. By increasing focal point position, depth of the hardened layer decreased. In sample F1 with a focal point position of 28 mm, depth of hardening was measured to be 130 µm from the macro metallographic image, and the maximum amount of hardness was 355 HV. While in sample F3 with a focal point position of 24 mm depth of hardening and maximum hardness were 199 µm and 444 HV respectively.

It could be explained by the concept of the incident beam area. The incident beam area is the area which the beam interacts with the material surface. When the focal plane distance

increases, the incident beam area also increases (See Figure 2-a). By increasing the incident beam area, the beam density reduced. Moreover, the energy transferred to the material will become less. Finally, it leads to lower hardness and lower depth of the hardened layer.

The effect of laser beam increased due to an increase in laser pulse energy, which resulted in more surface hardness and depth of penetration. Effect of laser pulse energy for samples E1, E2 and E3 is shown in Figure 5.

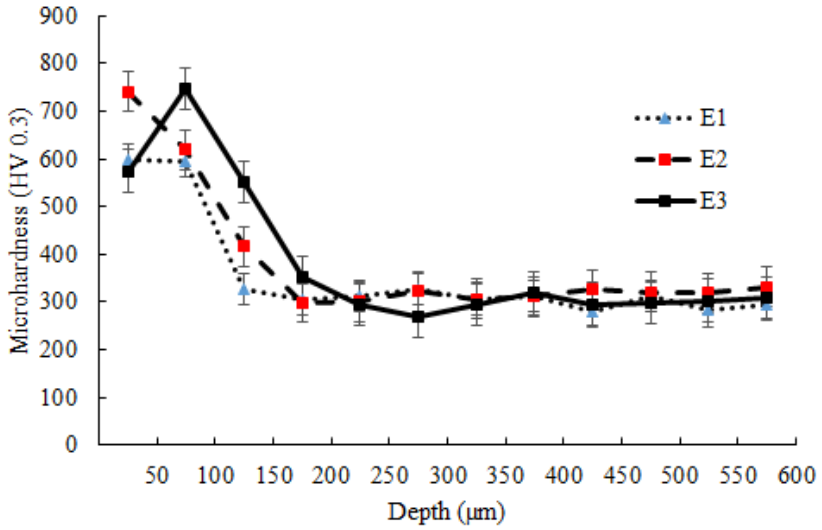

Fig. 5 Microhardness profile in depth of the laser-hardened layer in laser pulse energy tests

In sample E4 with a pulse energy of 14.7 J, depth of hardness was measured to be 142 µm, while sample E2 with a higher pulse energy of 16.8 J gave a depth of 350 µm. Therefore, it is concluded that the higher the pulse energy, the higher the depth of the hardened layer.

Comparative diagram between selected samples for E and F series is shown in Figure 6. The sample E2 has a higher depth and hardness rather than the other samples. It is due to less pulse width in constant peak power which could create sharper pulses and increase the effect of the laser beam.

It is noticeable that for sample E2 as shown in Figure 7 mark of the first Vickers indenter is visible in delta ferrite phase which has less hardness in comparison with the adjacent martensite phase. Increase in hardness up to 747 HV due to an increase in laser energy in sample E2 is shown in Figure 6. Also, the depth of hardness was determined 350 µm. In sample E3 which had less pulse energy about 15.75 J, the maximum amount of hardness and depth were 598 HV and 211 µm, respectively.

By moving from the surface toward the depth of the sample, hardness reduced equal to base metal hardness; it means more energy affects the surface.

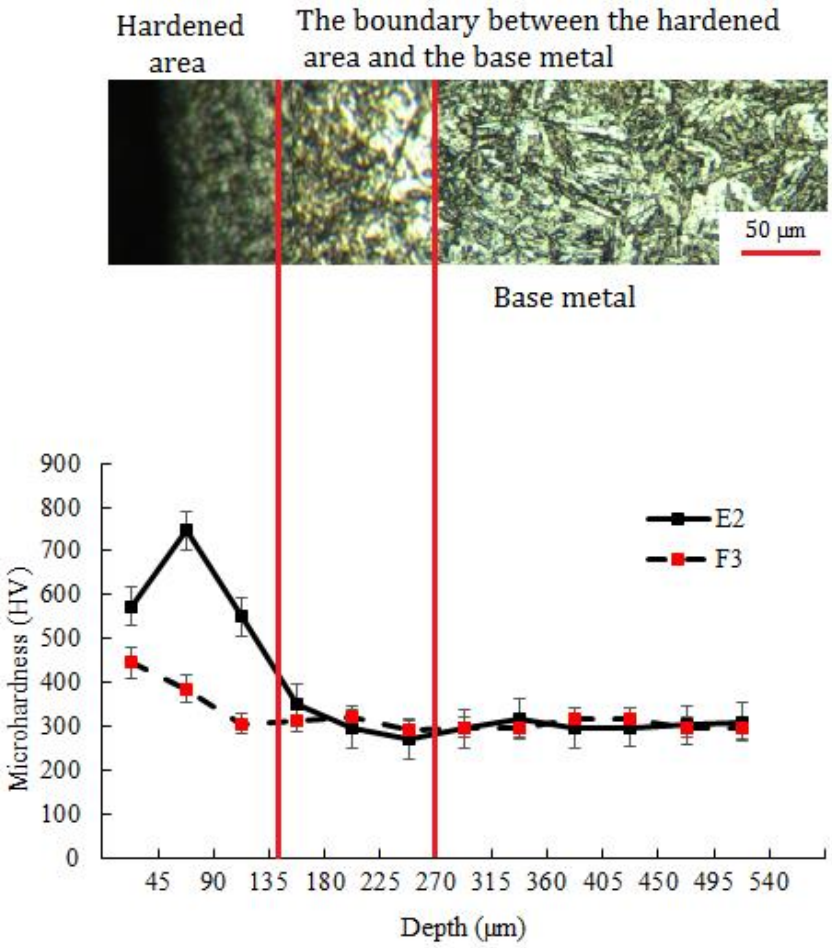

Fig. 6 Microhardness profile in depth of the laser-hardened layer for E2 and F3 samples

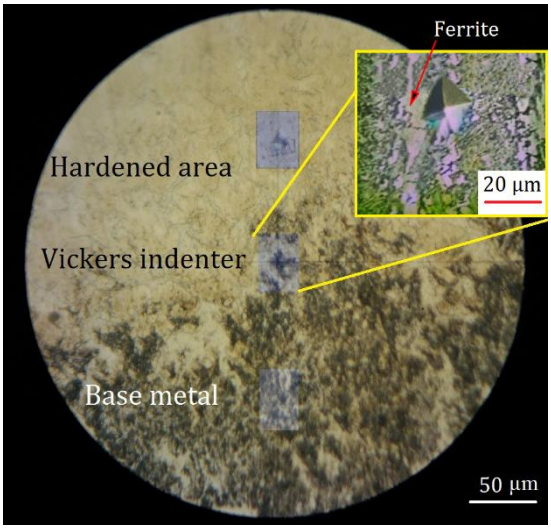

Fig. 7 Vickers indenter mark in the delta ferrite phase

As shown in Figure 8, surface hardness decreased due to an increase in distance between the laser and the surface, which is because of an energy intensity reduction and therefore the surface hardened less and vice versa. The focal plane position for samples F2, F3, and F4 are

26 mm, 24, and 22 mm, respectively. So by reduction the focal plane position the energy density of the laser is increased which leads to transfer more heat energy to the material surface. It causes more martensite phase transformation and therefore a higher surface hardness in sample F4 in comparison with two other samples.

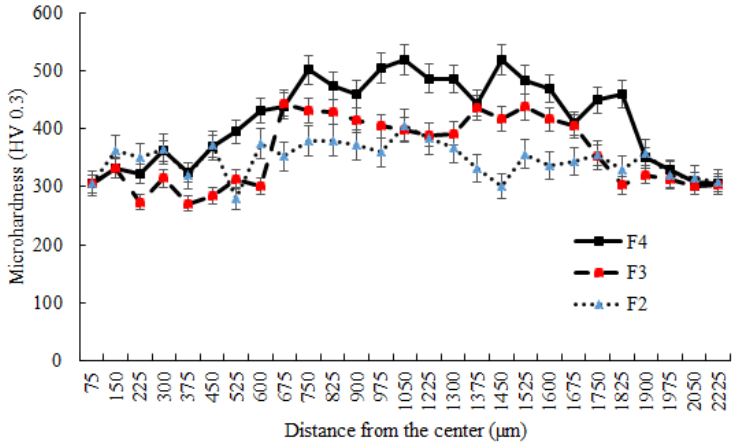

Fig. 8 Microhardness profile in width of the laser-hardened layer

By comparing Figures 2 and 8, according to explanations of Figure 2(a), the resemblance of microhardness distribution on the sample surface and Gaussian distribution of laser is sensible. It is possible to find a relation between these microhardness values along the width of the hardened area with a Gaussian distribution, which shows how laser penetrate the matter and how the Gaussian distribution of beam is on the surface of the sample. In sample F4 which laser had a very small distance with surface more hardness achieved, and center of the beam had higher energy which has a direct relationship with hardness value and its distribution. Whereas in sample F2 the distance between laser and surface increased in comparison with other samples, hardness value decreased. It can be explained by the effect of laser focal point position which by increasing this value, less energy will affect the surface (because focusing at a specific point is reduced). Changes in laser pulse energy led to noticeable effects on hardness value and also the depth of penetration. In Figure 9 effect of pulse energy changes on hardness in width of the hardened layer for samples E1 to E3 is shown.

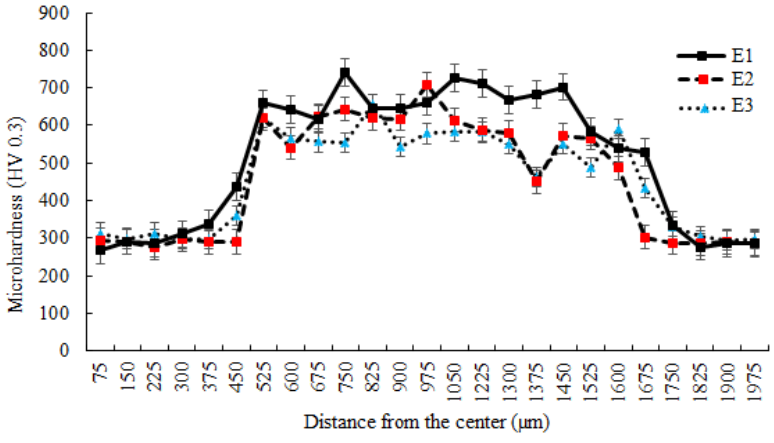

Fig. 9 Microhardness profile in width of the laser-hardened layer in E series

In sample E2 which had the highest pulse energy of 16.8 J the hardness value determined to be 747 HV. In sample E1 because of higher laser energy interacting with steel surface in respect to samples E2 and E3, there is less ferrite phase. Therefore Vickers indenter shows higher hardness due to more homogeneous martensite phase in sample E1.

3-3 Microstructure study of hardened layer

Figure 10 shows the homogeneous martensite structure of examined AISI 410 martensitic stainless steel. The studied material was warm worked, air quenched AISI 410 martensitic stainless steel; therefore, there is a noticeable delta ferrite phase in the martensitic base. Delta ferrite phase forms at the quenching stage for quenched tempered steels [24]. After production, if steel quenches rapidly in air or water, delta ferrite will not form [25-27].

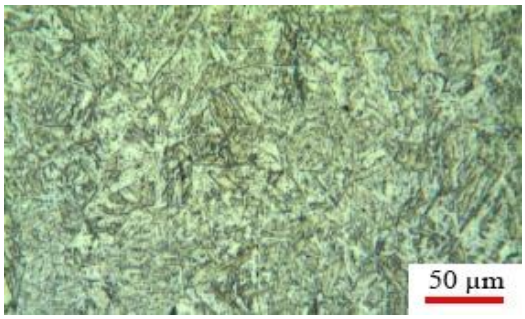

Fig. 10 Microstructure of base martensitic stainless steel AISI 410

In this part, the microstructure of the sample with the best conditions (maximum hardness and depth of penetration) for each variable parameter, i.e., laser pulse energy and focal point position has studied. Figure 11-a shows the microstructure of the hardened surface of sample F4, where more ferrite phase observed in comparison with sample E1. It is evident in Figure 11-b that martensite phase formed in the surface of the steel which leads to increases in surface hardness in this area.

When Vickers indenter goes through delta ferrite phase, measured hardness was less than the hardness of adjacent area. In sample E1 due to more interaction between laser and surface of AISI 410 martensitic stainless steel, the measured hardness was higher. Because of increasing power and decreasing focal point position, more martensite phase appeared which led to higher surface hardness.

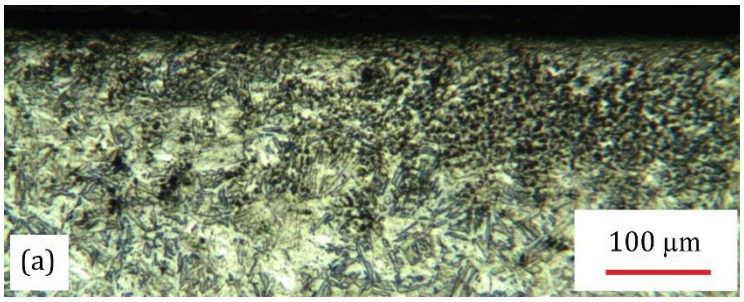

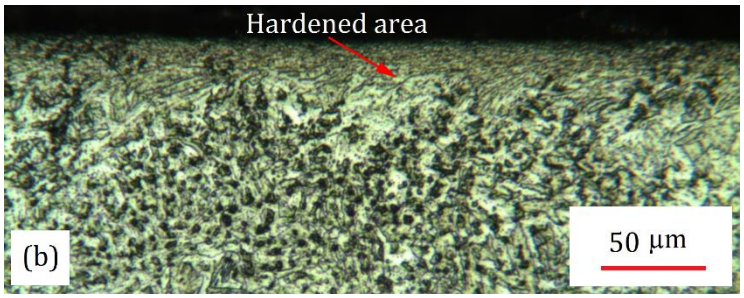

Fig. 11 The microstructure of laser hardened zone of martensitic steel AISI 410 for sample F4 a) magnitude of 100X b) magnitude of 200X

Metallographic images of sample E1 after laser hardening process for the hardened surface, an intermediate layer (a layer between the hardened surface and the base metal) and base metal under the hardened area is shown in Figure 12. In hardened surface, fine martensite and delta ferrite phases are scattered (Figure 12-a). Because of rapid quenching and lack of time for dissolution, delta ferrite did not dissolve completely and remained in a hardened structure which decrease the hardness value of these areas [28, 29]. As shown in Figure 12-a, in the laser-hardened area the amount of delta ferrite phase of sample E1 is less than other samples. In Figure 12-b, the hardened surface of AISI 410 is shown, which include martensite and delta ferrite phases. Figure 12-c shows the intermediate layer. The hardened part with a curve shape separated from the base metal which not affected by the laser. The base metal beneath the hardened layer is shown in Figure 12-d.

By comparing Figure 12 with Figure 10 (base metal), it is concluded that phase transformation has not taken place in the steel under the hardened layer, which means that this area has not been affected by the laser. Hardness is almost constant in length of the laser line, but in width, hardness value fluctuates due to the existence of delta ferrite phase in martensitic base [30]. In general, hardness is higher at the center line and gradually decreased along width up to base metal hardness.

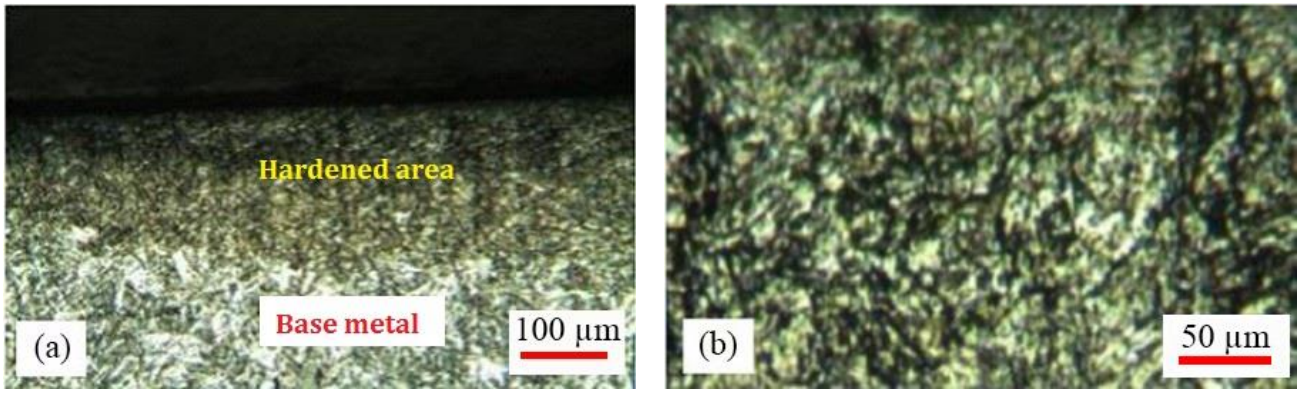

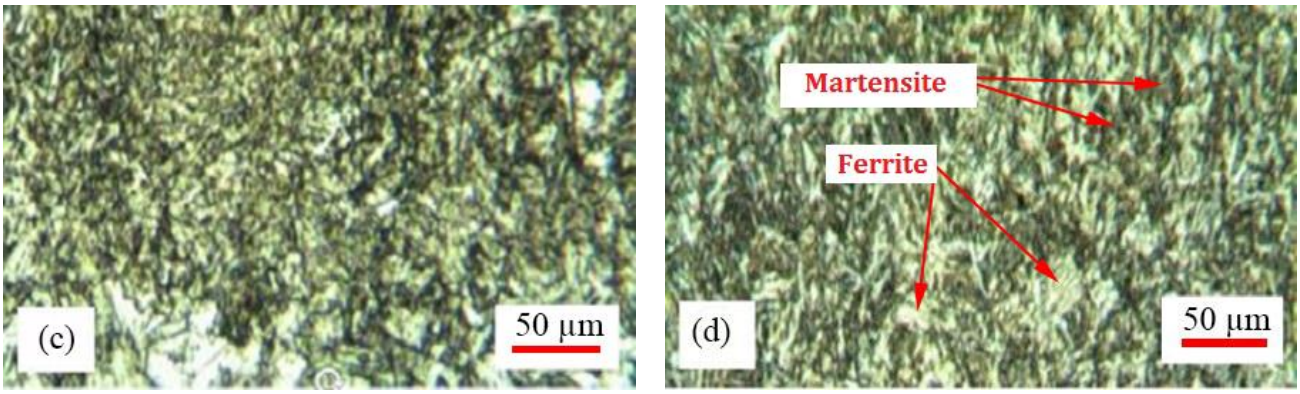

Fig. 12 The microstructure of laser hardened zone of AISI 410 for sample E1 a) microstructure of the all hardened zone b) microstructure of the top surface of hardened layer c) microstructure of the middle zone of hardened layer d) microstructure of the base metal under the hardened zone

To study the base and hardened AISI 410 microstructure, more precisely FE-SEM images were taken from the cross-sections. FE-SEM images of samples F3 and E1 are shown in Figure 13, which ferrite phase observed in the martensite base. As shown in Figure 13-b, ferrite particles were heat treated due to the high energy input of Nd:YAG laser. According to Figure 13, it is evident that fine grain martensite and ferrite phase are distributed in the microstructure. The reason is the high cooling rate and lack of time for complete dissolution of the ferrite particles. Figure 13-b shows the distributed ferrite in the microstructure of the hardened zone. Also, the retained austenite and carbide phases in hardened area from sample E1 are observable in Figure 13-c and d, respectively.

It is mentioned in the literature that corrosion behavior of martensitic stainless steels depends on two microstructural factors, including a) amount and size of carbides and b) retained austenite [31]. Carbides are rich in chromium element in steels with high chromium content because chromium has a high tendency for forming carbide phase [32-33]. The more the carbides in the structure, the more the trapped chromium in carbides, which reduces the remained chromium for forming a passive layer, therefore, the corrosion resistance decreased. Also, the carbides with bigger sizes have destructive effects on corrosion resistance because of more heterogeneity in the structure. On the other side, due to the higher resistance of austenite against corrosion rather than martensite; therefore, retained austenite will improve corrosion resistance [34]. One of the reasons for improving the corrosion resistance of stainless steels after laser hardening is mentioned to be cleaning the surface from undesirable impurities [35].

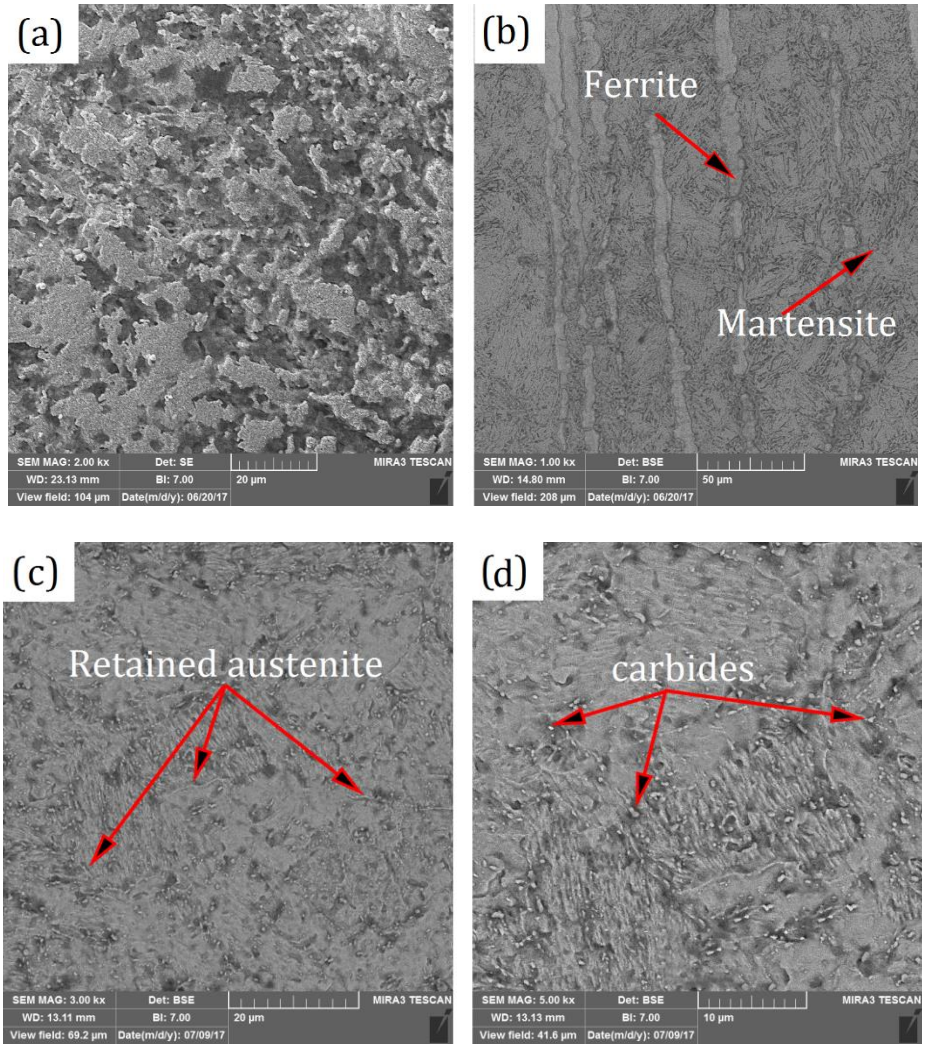

Fig. 13 FESEM images of a) 410 SS base material, b) hardened area of sample F3, c, d) hardened area of sample E1.

XRD graphs of the base metal and laser hardened zone for AISI 410 martensite stainless steel is shown in Fig. 14. By analyzing and investigation the XRD graphs of the AISI 410 and steel, the Martensite-Ferrite phases, and also the Martensite-Ferrite-Carbide phases, are observable respectively. As can be seen, the XRD graphs confirm the presence of ferrite particles for AISI 410 steel. Fig. 14 shows that the ferrite and martensite phases in the hardened zone of AISI 410 are smaller than of raw materials.

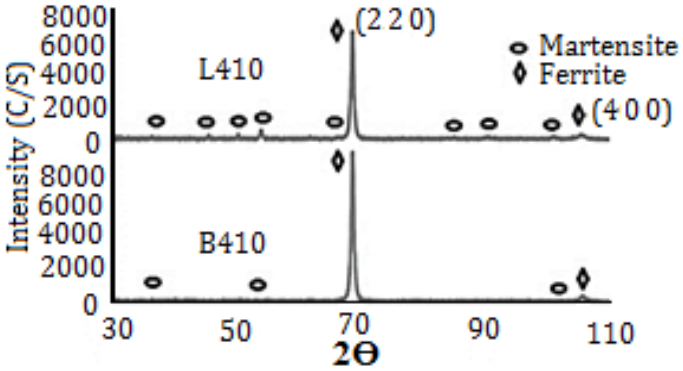

Fig. 14 images of XRD graphs for the as-received and the laser hardened zone

3-4 Corrosion analysis

In potentiodynamic polarization tests potential graphed versus current density which respectively demonstrates the thermodynamic and kinetic tendency of corrosion phenomenon. As corrosion potential goes toward more noble values and corrosion current density reduces, the thermodynamic tendency of corrosion and also corrosion rate will decrease [36, 37]. This trend is shown in Figures 15 and 16.

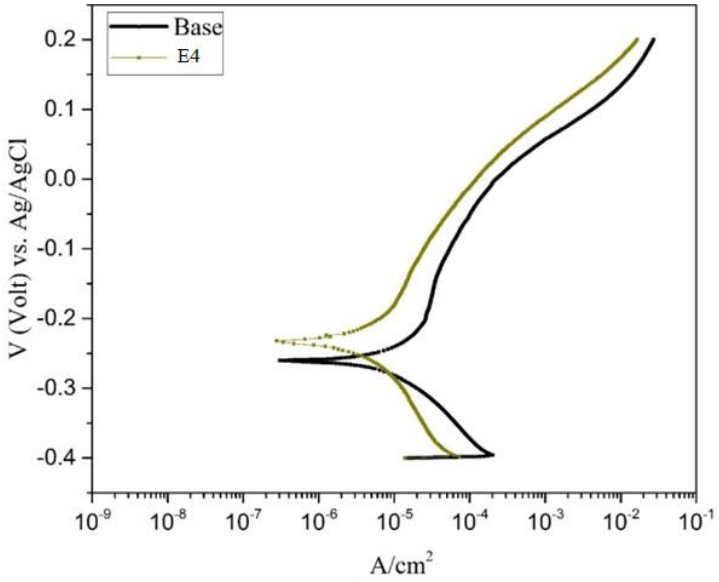

Fig. 15 Comparative polarization diagram of samples E4 and base

Extracted corrosion current density (i_{corr}) of E and F series samples from their polarization curves are shown in Tables 4 and 5.

Table 4. Corrosion current density data for E series samples

Samples	base	E1	E2	E3	E4
i_{corr}(A/cm^2)	4.63	3.6	6.244	1.948	1.806

From obtained corrosion test results, in E series samples the best corrosion behavior showed for sample E4 (Table 4). Improved corrosion resistance of sample E4 was due to the reduction of laser energy that finally resulted in more retained austenite in this sample. Also, in E series samples the lowest hardness value due to less martensite phase was for E4 which this issue confirms its corrosion resistance due to more retained austenite.

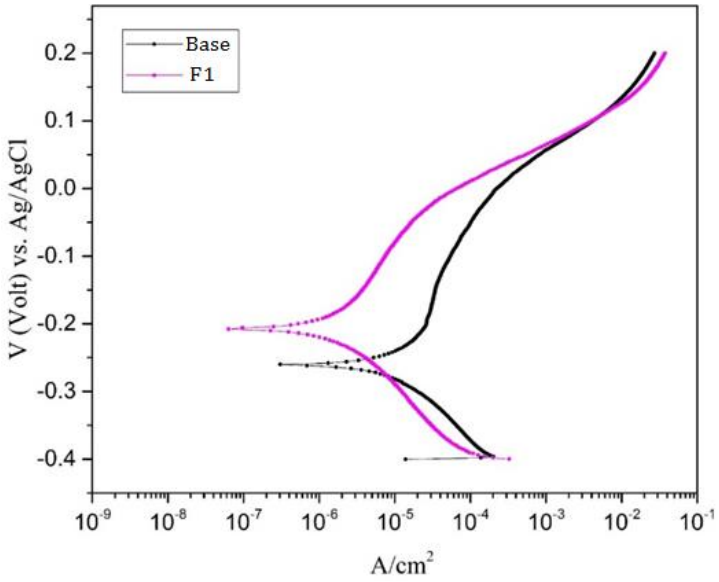

Fig. 16 Comparative polarization diagram of samples F1 and base

The best corrosion resistance in F series samples was for sample F1. According to Figure 16 and Table 5, for this sample potential goes toward positive values and corrosion current density decreased to a value of about ¼ times the value for the base sample. Therefore, increasing laser focal point position in sample F1 resulted in more retained austenite, lower hardness value and higher resistance against corrosion. For corrosion resistance, durable, long-lasting applications metal treatment similar to the F series samples is preferred. However, for wear-resistant applications metal treatment similar to the E series samples is favored.

Table 5. Corrosion current density data for F series samples

Samples	base	F1	F 2	F3
i_{corr}(A/cm^2)	4.63	1.288	2.96	3.088

4- Conclusion

In this work, the effect of process parameters of Nd:YAG laser surface hardening of AISI 410 is investigated. According to experimental works, the following results concluded:

1. By increasing the laser focal point position, due to laser beam divergence, laser energy and consequently hardness and depth of penetration were reduced.
2. In the highest focal point position, the more corrosion resistance with a corrosion current density of 1.288 A/cm^2 was obtained.
3. The highest corrosion resistance occurred in the lowest pulse energy which leads to increase in the amount of retained austenite and decreases in the hardness.
4. The maximum hardness value of AISI 410 obtained to be 762 HV with 460 µm depth.
5. Lack of undesirable surface impurities, reducing the size and amount of carbides and increasing the retained austenite cause to increase in corrosion resistance.

5- References:

[1] M. Moradi, M. K. Moghadam, M. Kazazi, Improved Laser Surface Hardening of AISI 4130 Low Alloy Steel with Electrophoretically Deposited Carbon Coating. Optik 2019; 178: 614-622.

[2] M. Moradi, M. K. Moghadam, High power diode laser surface hardening of AISI 4130; statistical modelling and optimization. Optics and Laser Technology 2019; 111: 554-570.

[3] B. Mahmoudi, M. J. Torkamany, R. Sabour Rouh Aghdam, J. Sabbaghzade, Laser surface hardening of AISI 420 stainless steel treated by pulsed Nd: YAG laser. Materials & Design 2010; 31(5): 2553-2560.

[4] Al-Sayed, S., et al., Characterization of a Laser Surface-Treated Martensitic Stainless Steel. Materials 2017; 10(6): 595.

[5] G. Zirehpour, R. ShojaRazavi, E. Moayerifar, Evaluating Wear Properties of AISI 420 Martensitic Stainless Steel after Laser Transformation Hardening. International Journal of Iron & Steel Society of Iran 2012; 9(2): 5-8.

[6] Jahromi, S.J., A. Khajeh, and B. Mahmoudi, Effect of different pre-heat treatment processes on the hardness of AISI 410 martensitic stainless steels surface-treated using pulsed neodymium-doped yttrium aluminum garnet laser. Materials & Design, 2012. 34: 857-862.

[7] Krishna. B. V, A. Bandyopadhyay, Surface modification of AISI 410 stainless steel using laser engineered net shaping (LENS TM). Materials & Design 2009; 30(5): 1490-1496.

[8] F. Cordovilla, A. Garcia-Beltran, P. Sancho, J. Dominguez, L. Ruiz-de-Lara, J. L. Ocana, Numerical/experimental analysis of the laser surface hardening with overlapped tracks to design the configuration of the process for Cr-Mo steels. Materials & Design 2016; 102: 225-237.

[9] D. Badkar, K. Pandey, G. Buvanashekaran, Effects of laser phase transformation hardening parameters on heat input and hardened-bead profile quality of unalloyed titanium. Transactions of Nonferrous Metals Society of China, 2010; 20(6): 1078-1091.

[10] C. Soriano, Effect of laser surface hardening on the microstructure, hardness and residual stresses of austempered ductile iron grades. Applied Surface Science 2011; 257(16): 7101-7106.

[11] Jong-Do, K., et al., Laser transformation hardening on rod-shaped carbon steel by the Gaussian beam. Transactions of Nonferrous Metals Society of China, 2009. 19(4): p. 941-945.

[12] Lo, K., F. Cheng, H. Man, Laser transformation hardening of AISI 440C martensitic stainless steel for higher cavitation erosion resistance. Surface and Coatings Technology 2003; 173(1): 96-104.

[13] Babu, P. D, G. Buvanashekaran, K.R. Balasubramanian, Experimental studies on the microstructure and hardness of laser transformation hardening of low alloy steel. Transactions of the Canadian Society for Mechanical Engineering, 2012; 36(3): 242-257.

[14] I. A. Pinahin, V. A. Chernigovskij, A. A. Bracihin, M. A. Yagmurov, Improvement of wear resistance of VK6, VK8, T5K10, and T15K6 hard alloys by volume pulsed laser hardening. Journal of Friction and Wear; 2015. 36(4): 330-333.

[15] N. K. Othman, S. Yahya, M. C. Ismail, Corrosion inhibition of steel in 3.5% NaCl by rice straw extract. Journal of Industrial and Engineering Chemistry 2018; In press.

[16] Sh. Chen, D. Zhang, Study of corrosion behavior of copper in 3.5 wt.% NaCl solution containing extracellular polymeric substances of an aerotolerant sulphate-reducing bacteria. Corrosion Science 2018; 136: 275-284.

[17] Laser Institute of America, Handbook of Laser Materials Processing. Magnolia Publishing Inc (2001).

[18] G. HabedankJ. WoitschigT. Seefeld, Pulsed laser hardening of component-like specimens Part 1: Procedures, properties and their simulation, Haerterei-Technische Mitteilungen 2005; 60(4): 195-206.

[19] Asm metals handbook, Metallography and microstructures, The materials information company1992; 9.

[20] Y. Zhang, Ch. Ding, L. Pan, Y. Cai, Laser arrays of partially coherent beams with multi-Gaussian correlation function. Journal of Quantitative Spectroscopy and Radiative Transfer 2018; 218: 1-11.

[21] Cong Sun, Jinchao Duan, Dongxue Lan, Zhenxin Liu, Shichao Xiu, Prediction about ground hardening layers distribution on grinding chatter by contact stiffness, Archives of Civil and Mechanical Engineering 2018; 18(4): 1626-1642.

[22] Yong Xiang, Deping Yu, Fangyuan Liu, Cheng Lv, Jin Yao, Determining the heat flux distribution of laminar plasma jet impinging upon a flat surface: An indirect method using surface transformation hardening, International Journal of Heat and Mass Transfer 2018; 118: 879-889.

[23] Mehrshad Mehrpouya, Annamaria Gisario, Andrea Brotzu, Stefano Natali, Laser welding of NiTi shape memory sheets using a diode laser, Optics & Laser Technology 2018; 108: 142-149.

[24] Harry Chandler, Heat Treater's Guide, Practices and procedures for nonferrous alloys, the materials information company (1996).

[25] M. Moradi, H. Arabi, S. J. Nasab, K. Y. Benyounis, A comparative study of laser surface hardening of AISI 410 and 420 martensitic stainless steels by using diode laser. Optics and Laser Technology 2019; 111: 347-357.

[26] Beatriz Hortigón, José M.Gallardo, Enrique J.Nieto-García, José A.López, Strain hardening exponent and strain at maximum stress: Steel rebar case, Construction and Building Materials 2019; 196: 175-184.

[27] Olexandr Grydin, Anatolii Andreiev, Martin Joachim Holzweißig, Christian Johannes Rüsing , Kristina Duschik, Yaroslav Frolov, Mirko Schaper, Short Austenitization Treatment with Subsequent Press Hardening: Correlation Between Process Parameters, Microstructure and Mechanical Properties, Materials Science and Engineering: A Available online 8 February 2019.

[28] L. R. Migliore, Laser materials processing. Manufacturing engineering and materials processing (1996).

[29] F. Klocke, A. Demmer, A. Zaboklicki, Investigation into the use of high power diode lasers for hardening and thermal conduction welding. Proc. SPIE 1997; 592–598.

[30] M. Haag, T. Rudlaff, Assessment of different high power diode lasers for materials processing. Proc. SPIE 3097 1997; 583–591.

[31] Aiming, F., L. Jinming, and T. Ziyun, An investigation of the corrosive wear of stainless steels in aqueous slurries. Wear 1996; 1(193): 73-77.

[32] C. T. Kwok, K. H. Lo, F. T. Cheng, H. C. Man, Effect of processing conditions on the corrosion performance of laser surface-melted AISI 440C martensitic stainless steel. Surface and Coatings Technology 2003; 166(2): 221-230.

[33] Y. Samih, G. Marcos, N. Stein, N. Allain, E. Fleury, C. Dong, T. Grosdidier, Microstructure modifications and associated hardness and corrosion improvements in the AISI 420 martensitic stainless

steel treated by high current pulsed electron beam (HCPEB). Surface and Coatings Technology 2014; 259: 737-745.

[34] A.G. Olabi, R. Lostado-Lorza, K.Y. Benyounis, Review of Microstructures, Mechanical Properties, and Residual Stresses of Ferritic and Martensitic Stainless-Steel Welded Joints, in: Book: Comprehensive Materials Processing, May 2014.

[35] A.G. Olabi, M.s.J. Hashmi, Effects of the stress-relief conditions on a martensite stainless steel welded component, J. Mater. Process. Technol. 1998; 300 (3): 216–225.

[36] C. T. Kwok, K.H. Lo, , Fai Tsun Cheng, H.C. Man, Effect of processing conditions on the corrosion performance of laser surface-melted AISI 440C martensitic stainless steel. Surface and Coatings Technology, 2003; 166 (2): 221-230.

[37] Y.Samih, G.Marcos, N.Stein, N.Allain, E.Fleury, C.Dong, T.Grosdidier, Microstructure modifications and associated hardness and corrosion improvements in the AISI 420 martensitic stainless steel treated by high current pulsed electron beam (HCPEB). Surface and Coatings Technology, 2014; 259: 737-745.